

# Accurate retrieval of asymmetry parameter for large and complex ice crystals from in-situ polar nephelometer measurements

Guanglang Xu<sup>1</sup>, Martin Schnaiter<sup>1</sup>, and Emma Järvinen<sup>1</sup>

<sup>1</sup>Karlsruhe Institute of Technology

November 23, 2022

## Abstract

The retrieval of the asymmetry parameter from nephelometer measurements can be challenging due to the inability to detect the whole angular range. Here, we present a new method for retrieving the asymmetry parameter of ice crystals with relatively large size parameters ( $>50$ ) from polar nephelometer measurements. We propose to fit the angular scattering measurement with a series of Legendre polynomials and the best fitted coefficients give the asymmetry parameter. The accuracy of the retrieval is analyzed by accessing the smoothness of the phase function, which is closely linked to the complexity of ice particle. It is found that the uncertainty of retrieval could be smaller than 0.01, provided the measured intensity profile is smooth enough. As an application, we report an case study on Arctic cirrus, which shows a mean value for the asymmetry parameter of 0.72.

1           **Accurate retrieval of asymmetry parameter for large**  
2                   **and complex ice crystals from in-situ polar**  
3                           **nephelometer measurements**

4                   **Guanglang Xu<sup>1</sup>, and Martin Schnaiter<sup>1</sup>, Emma Järvinen<sup>1</sup>**

5                           <sup>1</sup>Karlsruhe Institute of Technology, Karlsruhe, Germany

6           **Key Points:**

- 7           • A new algorithm is developed for retrieving the asymmetry parameter of large and  
8           complex ice crystals from polar nephelometer measurements.  
9           • Accuracy of retrieval could be better than 0.01, provided sufficient smoothness of  
10          the phase function.  
11          • A case study of Arctic cirrus measurement during the CIRRUS-HL campaign is  
12          reported.

---

Corresponding author: Guanglang Xu, Emma Järvinen , [guanglang.xu@kit.edu](mailto:guanglang.xu@kit.edu),  
[emma.jaervinen@kit.edu](mailto:emma.jaervinen@kit.edu)

## 13 Abstract

14 The retrieval of the asymmetry parameter from nephelometer measurements can  
 15 be challenging due to the inability to detect the whole angular range. Here, we present  
 16 a new method for retrieving the asymmetry parameter of ice crystals with relatively large  
 17 size parameters ( $> 50$ ) from polar nephelometer measurements. We propose to fit the  
 18 angular scattering measurement with a series of Legendre polynomials and the best fit-  
 19 ted coefficients give the asymmetry parameter. The accuracy of the retrieval is analyzed  
 20 by accessing the smoothness of the phase function, which is closely linked to the com-  
 21 plexity of ice particle. It is found that the uncertainty of retrieval could be smaller than  
 22 0.01, provided the measured intensity profile is smooth enough. As an application, we  
 23 report an case study on Arctic cirrus, which shows a mean value for the asymmetry pa-  
 24 rameter of 0.72.

## 25 Plain Language Summary

26 The asymmetry parameter of ice crystals is a parameter that can largely determine  
 27 cirrus cloud's interaction with solar radiation energy, and therefore its magnitude is im-  
 28 portant for climate and weather prediction models. In-situ measurements using neph-  
 29 elometers is a direct way to measure partial angular scattering functions, and the accu-  
 30 racy of these measurements is of utmost importance. In this paper, we report a novel  
 31 method for retrieving the asymmetry parameter from polar nephelometer measurements.  
 32 Depending on the smoothness of the measured angular scattering function, the accuracy  
 33 of the retrieval could be very high. We report a case study over the Arctic region, show-  
 34 ing a low asymmetry parameter around 0.72.

## 35 1 Introduction

36 When solar radiation reaches the Earth's atmosphere, it is likely that the radia-  
 37 tion is interacting with cirrus clouds, as they are formed in high altitudes and have a large  
 38 coverage. It is recognized that cirrus's interaction with solar and infrared radiation will  
 39 play a significant role in the energy balance of the Earth-atmosphere system (Liou, 1986,  
 40 1992; Stephens et al., 1990). At visible wavelengths, the radiative properties of cirrus are  
 41 mainly determined by the ice crystal light scattering properties. Particularly, these prop-  
 42 erties define which fraction of the incoming radiation is redirected back into space and  
 43 is therefore lost for the energy budget of the Earth. Hence, the so-called asymmetry pa-  
 44 rameter, characterizing the relative difference of the forward and backward scattered en-  
 45 ergy, needs to be determined. Although it contains only partial information of the an-  
 46 gular scattering function, the asymmetry parameter is a key input parameter for the two-  
 47 stream approximation of radiative transfer models (Liou, 2002). Because climate mod-  
 48 els mostly apply two-stream or Eddington approximations to parameterize radiative trans-  
 49 fer (Fouquart et al., 1991; Randles et al., 2013), the asymmetry parameter of cirrus clouds  
 50 largely determines their radiative impact in climate models (Kristjánsson et al., 2000;  
 51 Fu, 2007; Liou, 2002).

The significance of the asymmetry parameter for cirrus clouds is also manifested  
 by its connection to remote sensing (Yang et al., 2018; C.-Labonnote et al., 2000). This  
 can be revealed by a simple approximation formula of the plane-albedo of thin clouds  
 (Liou, 2002; Meador & Weaver, 1980), i.e.,

$$R = \frac{\omega_0}{2\mu_0}(1 - g)\tau, \quad (1)$$

52 where  $\tau$  is the optical thickness,  $\omega_0$  is the scattering albedo,  $\mu_0$  is the cosine of direction  
 53 of the incident solar radiation, and  $g$  is the asymmetry parameter of clouds. Because the  
 54 optical depth is retrieved by measuring the reflected radiance for passive remote sens-

ing, the assigned value of  $g$  (model value) for clouds, if not accurate, could induce large biases to the retrieval of optical thickness.

The asymmetry parameter of spherical particles, like water droplets, can be computed analytically due to their simplicity of shape. In contrast, ice crystals often exhibit complex shapes with a high degree of non-sphericity. This morphological complexity poses a great challenge for quantitatively studying their optical properties. Over the last few decades, progress has been made towards the improvement of the modeling capability of light scattering by non-spherical particles. Various techniques including the geometric-optics ray tracing and numerically accurate methods have been developed for modeling the light scattering properties of ice crystals (Macke et al., 1996; Yang & Liou, 1996b; Mishchenko et al., 1996; Yurkin et al., 2007; Taflove & Umashankar, 1990; Yang & Liou, 1996a). The merits of these methods include that they are theoretically sound, highly accurate, and have the abilities to predict and interpret observational data, particularly polarization data. However, the limitation that one has to make specific assumptions on the particle morphology often results in the use of idealized and simplified shapes, which most likely do not fully represent the optical properties of real atmospheric crystals with a high degree of morphological complexity.

Another approach for estimating the asymmetry parameter of cirrus clouds is to analyze the upwelling flux or multi-directional polarization data by applying radiation transfer theory and optical scattering models, e.g., (Stephens et al., 1990; Diedenhoven et al., 2012, 2013). The advantage of such analyses comprises the capability of probing cloud-top information, being most relevant to the reflectance of clouds. As an indirect estimation, however, important assumptions on the cloud geometry (i.e., plane-parallel structure) has to be made for such analysis to be valid.

The most direct way of deriving the asymmetry parameter for ice crystals is the in-situ measurement by a nephelometer. Several instruments have been developed to measure the angular light scattering of ice crystals in-situ, including the Polar Nephelometer (Gayet et al., 1998) (PN), the Cloud Integrating Nephelometer (CIN) (Gerber et al., 2000), and the Particle Habit Imaging and Polar Scattering (PHIPS) probe (Abdelmonem et al., 2016; Schnaiter et al., 2018). A common limitation of these instruments is the incapability to measure the whole angular range, particularly in the near-forward and near-backward scattering directions. Notably, by directly applying the cosine-weighted integral definition, (Gerber et al., 2000) use CIN measurements to estimate the asymmetry parameter of cloud elements. In their approach, a fraction of energy in the forward scattering direction must be assumed in accordance with light scattering (diffraction) simulations. Other methods involving angular scattering measurements often use the best-fitting approach, by comparison with specific light scattering models, to determine the asymmetry parameter of ice crystals.

Despite decades of research, the value of the asymmetry parameter for ice crystals has not been very well constrained. If one ask the question what is the value of the asymmetry parameter for cirrus clouds, experimentalists and modellers will probably give different answers. Tab. 1 shows some typical values of  $g$  obtained from measurements and modeling studies. In general, the radiometer-based studies from the early 90s give quite low values of  $g$ , the Cloud Integrating Nephelometer (CIN) measurements tend to give values around 0.74 – 0.75. A typical range of 0.76 – 0.78 is reported from Polar nephelometer (PN) measurements and the modelling studies normally predict the asymmetry parameter above 0.8. The discrepancies between model and observation still motivate extensive studies of cirrus cloud optical properties (Bacon & Swanson, 2000; Gerber et al., 2000) .

To further improve the accuracy of in-situ measurements, in this work, we developed a new method for retrieving the asymmetry parameter of ice crystals from polar nephelometer measurements with the PHIPS probe. The range of applicable size param-

**Table 1.** Values of asymmetry parameter ( $g$ ) estimated from measurement and modelling studies.

$g$ from radiometer/polarimeter observations	Reference
0.7	(Stephens et al., 1990)
0.7	(Stackhouse Jr & Stephens, 1991)
0.7	(Wielicki et al., 1990)
0.75	(Shiobara & Asano, 1994)
0.76-0.78	(Diedenhoven et al., 2012, 2013)
$g$ from the Cloud Integrating Nephelometer (CIN)	Reference
0.74 $\pm$ 0.03	(Gerber et al., 2000) (Garrett et al., 2001)
0.75 $\pm$ 0.01	(Garrett et al., 2003)
$g$ from Polar nephelometer (PN)	Reference
0.78-0.79	(Jourdan et al., 2003)
0.76-0.77	(Gayet et al., 2004)
0.76-0.77	(Shcherbakov et al., 2005)
0.77-0.78	(Mioche et al., 2010)
0.75	(Järvinen et al., 2018a)
$g$ from numerical models	Reference
0.79-0.88 (bullet rosettes)	(Iaquinta et al., 1995)
0.80-0.92 (plates).	(Macke et al., 1998)
0.77-0.86 (columns)	(Macke et al., 1998)
0.76-0.77 (two-habit model)	(Liu et al., 2014)

107 eters (ratio of the characteristic length to the wavelength) is where geometric-optics treat-  
 108 ments are applicable (Yang et al., 2013). In contrast to previous methods, our method  
 109 avoids specific assumptions for the undetectable angular range, which removes biases that  
 110 stem from the use of specific optical particle models.

111 The structure of this paper is as follows, in section 2, we revisit the basic princi-  
 112 ples of nephelometer measurement of asymmetry parameter. In section 3, we introduce  
 113 the methodology for measuring asymmetry parameter for PHIPS. In section 4, we an-  
 114alyze the errors associated with the method. Section 5 reports the results from a recent  
 115 in-situ measurements in Arctic cirrus clouds. Section 6 concludes this study.

## 116 2 Nephelometer measurements of the asymmetry parameter

The asymmetry parameter  $g$  is defined as the cosine-weighted integral of the scat-  
 tering phase function  $P(\theta)$ :

$$g = \int_0^\pi P(\theta)\cos(\theta)\sin(\theta)d\theta, \quad (2)$$

where  $\theta$  is the scattering angle. As  $\cos(\theta)$  has a maximum value of 1 at  $\theta = 0$  and a  
 minimum value  $-1$  at  $\theta = \pi$ ,  $g$  measures the relative difference between the forward-  
 scattered and backscattered energy. This integral definition motivates the development  
 of the Cloud Integrating Nephelometer (CIN) instrument (Gerber et al., 2000), measur-  
 ing the accumulated scattered energy over a limited angular range with and without a  
 “cosine mask”. Specifically, the asymmetry parameter can be deduced from CIN mea-  
 surements by the following expression:

$$g = f + \frac{cF - cB}{F + B}(1 - f), \quad (3)$$

117 where  $f$  is a constant number accounting for the energy within the forward-scattering  
 118 range  $\theta \leq 10^\circ$ ,  $cF$  and  $cB$  are the integrals of the “cosine-weighted” forward-scattering  
 119 and backscattered energy respectively, while  $F$  and  $B$  denote the integration of forward-  
 120 scattering and backscattered energy without the “cosine mask”. The advantage of the  
 121 method is that the integration of the side-scattering energy could be accurate regard-  
 122 less of the smoothness of phase function. Nonetheless, this simple design also comes with  
 123 some drawbacks. First, the error induced by the factor  $f$  is hard to quantify, because  
 124 real ice crystals could be underrepresented by the light scattering models due to mor-  
 125 phological complexities associated with different scales. Second, for each cloud type, one  
 126 has to assume a different value of  $f$ , which increase the complexity of the retrieval al-  
 127 gorithm. It should be noted that Eq. (3) can also be applied to retrieve asymmetry pa-  
 128 rameter from polar nephelometer measurements (Auriol et al., 2001).

129 Another approach for estimating the asymmetry parameter is to use statistical in-  
 130 version method (Jourdan et al., 2003). This method requires the building of a look-up  
 131 table based on light scattering simulations, which is essentially a best-fitting approach.  
 132 The merits of such approach include that it can generate multiple parameters simulta-  
 133 neously, such as extrapolated scattering phase function, extinction coefficient, asymme-  
 134 try parameter and scattering albedo. Nevertheless, the retrieved parameters will be in-  
 135 evitably biased toward the pre-computed look-up table.

136 It can be seen that the existing algorithms for estimating the asymmetry param-  
 137 eter of ice crystals rely on simulated optical properties of specific hexagonal models. The  
 138 limitation of such approach is obvious,i.e., as the level of complexity of real ice crystal  
 139 increases, the model may not be representative anymore. This will inevitably introduces  
 140 biases for the retrieval of asymmetry parameter, making the accuracy assessment intractable.  
 141 This limitation is unlikely to be resolved by simply improving the accuracy of measure-  
 142 ment. Instead, an algorithm that minimizes the dependence on light scattering simula-  
 143 tions needs to be designed, which is the main objective of this study.

### 144 3 Methodology

We start by expanding arbitrary phase function  $P(\theta)$  in terms of series of Legendre polynomials  $P_l(\cos(\theta))$ ,

$$P(\theta) = \sum_{l=0}^{\infty} (2l+1) \hat{c}_l P_l(\cos(\theta)), \quad (4)$$

where  $\hat{c}_l$  denotes the expansion coefficient of degree  $l$ . Due to the orthogonal property of Legendre polynomials, the expansion coefficient  $\hat{c}_l$  can be evaluated by the following integral,

$$\hat{c}_l = \frac{1}{2} \int_{-1}^1 P(\theta) P_l(\cos(\theta)) d(\cos(\theta)) \quad (5)$$

Let the phase function be normalized to  $4\pi$ , i.e.,

$$\int_0^{2\pi} \int_0^{\pi} P(\theta) \sin(\theta) d\theta d\phi = 4\pi, \quad (6)$$

it follows that

$$\hat{c}_0 = 1, \quad (7)$$

and  $\hat{c}_1$  equals to the asymmetry parameter,

$$\hat{c}_1 = g, \quad (8)$$

145 meaning that asymmetry parameter is the first moment of scattering phase function with  
146 respect to Legendre polynomial.

For ice crystals whose size is large compared to incident wavelength, geometric optics ray-tracing approximation can be applied to calculate the optical scattering properties (Macke et al., 1996; Yang & Liou, 1996b). The scattering phase function is contributed by two separate parts, the external diffraction and ray-tracing part. The ray-tracing part of scattering phase function, accounting for reflection and refraction of light rays, is what a polar nephelometer can measure practically. According to the principle of light scattering in geometric-optics regime, the diffraction and ray-tracing contribution will be asymptotically equal when particle size parameter becomes larger than 50 (Yang et al., 2013). For PHIPS probe, with a laser beam of wavelength 532 nm, this lower limit on particle size is round 26  $\mu m$ . In this range, the scattering phase function can be approximately written as,

$$P(\theta) = \frac{1}{2\omega_0} [(2\omega_0 - 1)P_{GO}(\theta) + P_D(\theta)], \quad (9)$$

147 where  $P_{GO}(\theta)$  denotes the geometric-optics ray-tracing contribution and  $P_D(\theta)$  is the  
148 external diffraction contribution, and  $\omega_0$  is the single scattering albedo. The well-known  
149 22-degree and 46-degree halo produced by pristine hexagonal cylinders are due to the  
150 contribution of  $P_{GO}(\theta)$ . More specifically, it can be explained by the light rays refracted  
151 through prism angles of 60 degree and 90 degree respectively. For complex real ice crystals,  
152 the phase function  $P_{GO}$  is generally featureless.  $P_D(\theta)$  can be calculated by an  
153 integral involving the geometric projection of the particle along the incident direction,  
154 resulting a highly forward-peaked phase function. Previously, to estimate the value of  $g$ ,  
155 a fraction of energy has to be assumed constant ( $\sim 0.56$ ) to account for the undetectable  
156 angular range of  $\theta < 10^\circ$ , which is dominated by diffraction contribution  $P_D(\theta)$  (Gerber  
157 et al., 2000).

Applying the Legendre expansion to Eq. (9), one can obtain the following relation for the corresponding expansion coefficients,

$$\hat{c}_l = \frac{1}{2\omega_0} [(2\omega_0 - 1)\hat{c}_{GO,l} + \hat{c}_{D,l}], l = 0, 1, 2, \dots \quad (10)$$

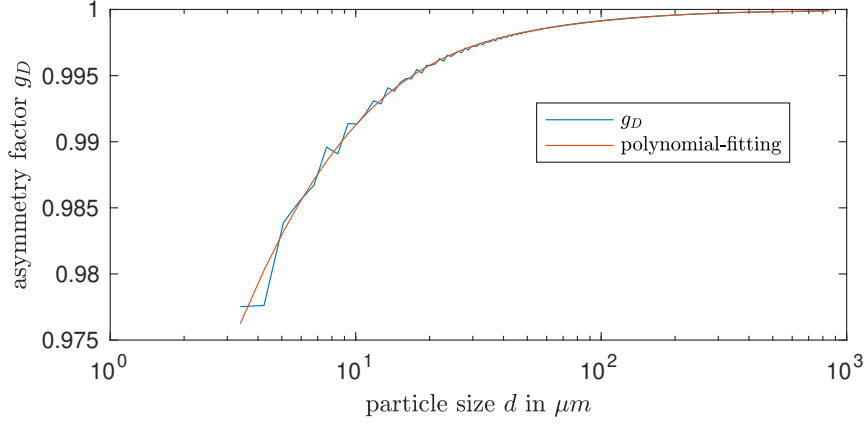


**Figure 1.** Asymmetry parameter  $g_D$  as a function of particle size  $d$ .

where  $\hat{c}_{GO,l}$  and  $\hat{c}_{D,l}$  are the expansion coefficients for geometric-optics and diffraction phase function respectively. Take  $l = 1$ , we have the relation for asymmetry parameter,

$$g = \frac{1}{2\omega_0} [(2\omega_0 - 1)g_{GO} + g_D], \quad (11)$$

where  $g_{GO} = \hat{c}_{GO,1}$  and  $g_D = \hat{c}_{D,1}$  are the asymmetry parameter contributed by geometric-optics and diffraction respectively. As the diffraction phase function is highly peaked,  $g_D$  is very close to unity. According to the analysis of scalar diffraction (SD) theory (Bohren & Huffman, 2008), the diffraction pattern for a spherical aperture shall have the following form:

$$P_{SD}(\theta) \propto (1 + \cos(\theta))^2 \left( \frac{J_1(x \sin(\theta))}{x \sin(\theta)} \right)^2, \quad (12)$$

where  $x$  is particle size parameter, and  $J_1$  is the first order Bessel function. According to the analysis in (Mishchenko et al., 2002), most of the diffracted energy will be confined into the angular range of  $\theta < 7/x$  (in radian), which is a small angular range for ice crystals that are large enough. Despite that the above analysis is valid for spherical particle, the error caused by non-spherical ice crystal should be small as well since the asymmetry parameter due to large particle diffraction is very close to unity. We therefore make the following assumption,

$$P_D(\theta) = P_{SD}(\theta). \quad (13)$$

To facilitate the retrieval, we computed the value of  $g_D$  as a function of particle size  $d$  in  $\mu m$  using Eq. (12), where  $d$  is defined as,

$$d = \frac{x\lambda}{\pi}, \quad (14)$$

158 where  $\lambda = 0.532 \mu m$  is the wavelength used for measurement. The results is displayed  
 159 in Fig. 1. On logarithmic scale,  $g_D(d)$  can be approximated by a polynomial of degree  
 160 4, i.e.,

$$g_D(d) = -5.9270 \times 10^{-5} - 0.00130 \times \ln(d) - 0.01087 \times (\ln(d))^2 + 0.04093 \times (\ln(d))^3 + 0.94029 \times (\ln(d))^4. \quad (15)$$

161 The above fitting uses particle size range from  $3.3 \mu m$  to  $846.7 \mu m$ , which covers most  
 162 the size range in our measurement. For particle being large than the upper limit, the value  
 163 at  $846.7 \mu m$  is used. In practice, the lower limit for Eq. (12) to be valid is assumed to

164 be  $26 \mu m$ . It can be seen that  $g_D$  is a weakly-varying function with respect to particle  
 165 size, resulting a relatively small error of 0.005 for the estimation of asymmetry param-  
 166 eter. Exploiting this weakly-varying feature of diffraction contribution is important, be-  
 167 cause we can mainly focus on analyzing the error due to the integration associated with  
 168 the geometric-optics phase function  $P_{GO}(\theta)$ , which will be discussed in the next section.  
 169 We note that van Diedenhoven (van Diedenhoven et al., 2014) also gives a empirical re-  
 170 lation between the  $g_D$  and size parameter  $x$  based on diffraction computation of hexag-  
 171 onal ice crystal of specific aspect ratio.

In the following, we shall find a set of Legendre polynomial coefficients up to de-  
 gree  $N_t$ , giving the best-fit to the measured angular intensities. By doing so, we auto-  
 matically obtain the asymmetry parameter  $g_{GO}$ . Let a series of coefficients denoted by

$$c_{\vec{GO}} = (c_{GO,0}, c_{GO,1}, c_{GO,2}, \dots, c_{GO,N_t}). \quad (16)$$

The problem can be cast as the following optimization problem:

$$\arg \min_{c_{\vec{GO}}} \sigma(c_{\vec{GO}}) := \sum_{n=1}^{N_m} \left( \sum_{l=0}^{N_t} c_{GO,l} P_l(\cos(\theta_n)) - I(\theta_n) \right)^2, \quad (17)$$

where  $I(\theta_n)$  is the measured intensity from the polar nephelometer at scattering angle  $\theta_n$ , and  $N_m$  is the total number of measurement directions. We then can obtain the nor-  
 malized coefficients and the asymmetry parameter by the following formula:

$$\hat{c}_{GO,l} = \frac{c_{GO,l}}{c_{GO,0}}, l = 0, 1, \dots, N_t. \quad (18)$$

The above optimization problem can be converted to a system of linear equations, and  
 solved by using least-squared-fitting formula, see e.g., (Hu et al., 2000). Nevertheless,  
 for arbitrary phase function to converge,  $N_t$  should be large enough. This could cause  
 numerical instability, as large matrix inversion will be involved. To circumvent this dif-  
 ficulty, we first compute the intensity  $I(\arccos(x_i))$  at Gauss-Legendre quadrature node  
 $x_i$  via interpolation and extrapolation of  $I(\theta_n)$ , and the coefficients of various degrees  
 can be then computed precisely via Gauss-Legendre quadrature integration:

$$c_{GO,l} = \frac{1}{2} \sum_{j=1}^{N_t} I(\arccos(x_j)) P_l(x_j) w_j, \quad (19)$$

172 where  $w_j$  are the weights with respect to the quadrature.

173 As suggested by Eq. (15), the asymmetry parameter, in other words, the first mo-  
 174 ment of diffraction phase function can be derived from Particle Size Distribution (PSD).  
 175 The PSD information is available from PHIPS probe since, besides recording single-particle  
 176 angular scattering functions, stereo-microscopic images are also recorded. Now we can  
 177 summarize our proposed method in the following flowchart:

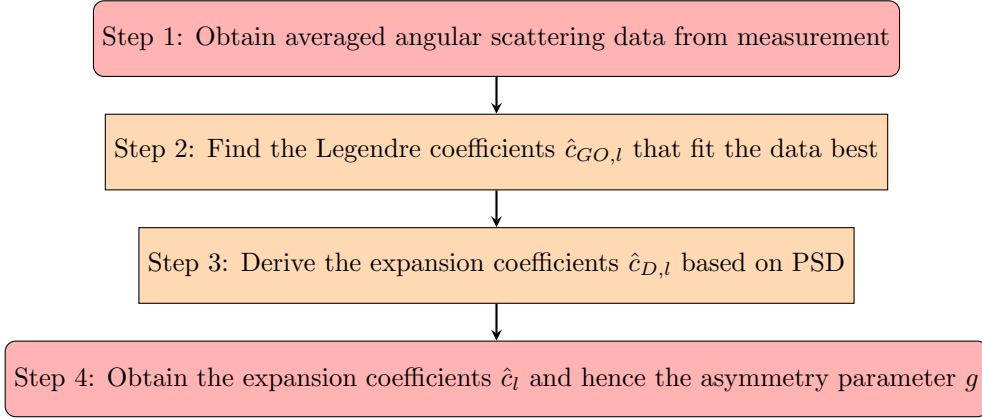


**Figure 2.** Method for retrieving asymmetry parameter from measurement

178 Note that by finding the expansion coefficients, we not only retrieve asymmetry pa-  
 179 rameter, but also recover the phase function at arbitrary scattering angle. In the next  
 180 section, we shall see that obtaining a set of best-fitting coefficients is crucial for analysing  
 181 the accuracy of retrieval.

The key ingredients of our method include two parts, one is the data fitting with Legendre polynomials, and second is the computation of diffraction expansion coefficients. Because the diffraction phase function is highly peaked, the expansion of such phase function requires many terms (could be larger than 6000). To circumvent this difficulty, one can approximate the diffraction pattern by the Henyey-Greenstein (H-G) phase function (van de Hulst, 1980), as the HG function is completely determined by the asymmetry parameter. In such way, the phase function expansion can be written as:

$$\hat{c}_l = \frac{1}{2\omega_0} [(2\omega_0 - 1)\hat{c}_{GO,l} + g_D(x)^l], l = 0, 1, 2, \dots, \quad (20)$$

182 It is interesting to see that Eq. (20) explicitly contains many parameters that are rel-  
 183 evant to light scattering, the asymmetry parameter, scattering albedo  $\omega_0$ , and size pa-  
 184 rameter  $x$ . Implicitly,  $\hat{c}_{GO,l}$  are largely determined by the particle morphology. These  
 185 coefficients are useful in radiative transfer computation, and now they can be derived  
 186 from the polar nephelometer measurements.

## 187 4 Error analysis

188 We shall now discuss the accuracy of the method. In practice, multiple error sources  
 189 for the estimation of asymmetry parameter could exist, including factors that are asso-  
 190 ciated with instruments, noise of measurements, shattering and so on. As we are mainly  
 191 concerned with the problem of designing an algorithm, in this part, we will be focusing  
 192 on the errors that are associated with the algorithm described in the last section.

### 193 4.1 Integration error

194 The retrieval of asymmetry parameter from nephelometer is nothing but perform-  
 195 ing integration based on an incomplete angular-intensity profile. For polar nephelome-  
 196 ter measurement, interpolation of the intensity is necessary. It is apparent that the ac-  
 197 curacy of interpolating the intensities (i.e.,  $P_{GO}(\theta)$ ) will be largely determined by its char-  
 198 acteristics, such as whether a peak or sharp-change of intensity appears at small scat-  
 199 tering angle and the halos that appears in pristine hexagonal crystals. Despite that the

200 measured the phase function (e.g. 18 to 170 degree ) is very often featureless, it is un-  
 201 certain how much error will be induced by applying Eq.(19). A basic property of Gauss-  
 202 Legendre quadrature is that the integration is exact provided that the integrand can be  
 203 represented using polynomials of degree up to  $N = 2n_t - 1$ , where  $n_t$  is the number  
 204 of quadrature weights or nodes used. If  $N$  is a relatively small number, the quadrature  
 205 nodes could be well confined in the range of detection, resulting a highly accurate esti-  
 206 mation of asymmetry parameter. In the following, we shall exploit this fact for the pur-  
 207 pose of error estimation.

In accordance with Eq. (19) and Eq. (18), taking  $l = 1$ , we have the following ex-  
 pression for  $g_{GO}$ :

$$g_{GO} = \frac{\sum_{j=1}^{n_t} I(\arccos(x_j))x_j w_j}{\sum_{j=1}^{n_t} I(\arccos(x_j))w_j}. \quad (21)$$

It can be seen that the value of  $g_{GO}$  will be exact as long as the intensity  $I(\theta)$  can  
 be represented using polynomials of degree up to  $N = 2n_t - 2$ , because we have a term  
 $I(\arccos(x_j))x_j$  in the numerator. Accordingly,

$$I(\theta) = Const. \times \sum_{l=0}^N (2l+1)\hat{\alpha}_l P_l(\cos(\theta)), \quad (22)$$

where a *Constant* is assumed such that  $\hat{\alpha}_0 = 1$ . This constant is irrelevant for the anal-  
 ysis due to Eq. (21). The accuracy of integration must be limited by the accuracy of ap-  
 proximating  $I(\theta)$  using Eq. (22). In general, we can use the following term associated  
 with the last coefficient to access the accuracy of approximation,

$$\varepsilon = (2N+1)|\hat{\alpha}_N|. \quad (23)$$

Hence, given a small coefficient  $|\hat{\alpha}_N|$ , the error is proportional to  $(2N+1)$ . This suggests  
 that the method will obtain its best accuracy only if the expansion coefficient decays fast  
 enough to small magnitude. In other words, the decay rate of the expansion coefficient  
 is a determining factor for the integration to be accurate. As we shall see in a moment,  
 this feature has very close relation with the morphological complexity of ice crystals. Let  
 us require that:

$$\varepsilon \leq 0.001, \quad (24)$$

which leads to

$$|\hat{\alpha}_N| \leq \frac{0.001}{2N+1}. \quad (25)$$

We note that the upper limit of  $N$  is crucial for accessing the accuracy for PHIPS. This  
 is because the number of  $N$  directly determines the Gauss-Legendre nodes and weights  
 to be used in the integration. Remember that a common limitation of current polar neph-  
 elometers is that they are not able to measure the whole angular range. For PHIPS, the  
 detection range is from 18 degree to 170 degree with 20 detectors equally spaced. For  
 the integration to be accurate, the corresponding Gauss-Legendre nodes shall be mostly  
 within the range of detection. Fig. 3 displays the Gauss-Legendre quadrature weights  
 when different number of nodes are used. The two vertical lines indicate the detection  
 range of PHIPS. It is not difficult to see that the best scheme for PHIPS is to be able  
 to use no more than 8 nodes for integration, which lead to

$$N \leq 14. \quad (26)$$

And therefore,

$$|\hat{\alpha}_N| \leq 3.448 \times 10^{-6}. \quad (27)$$

208 In other words, for PHIPS, if the measured intensity profile can be approximated by Eq.  
 209 (22) with  $N = 14$ , to such an extent that its expansion coefficient  $\hat{\alpha}_l$  decays to a mag-  
 210 nitude of  $3.448 \times 10^{-6}$ , the error associated with the asymmetry parameter should be  
 211 around the order of 0.001.

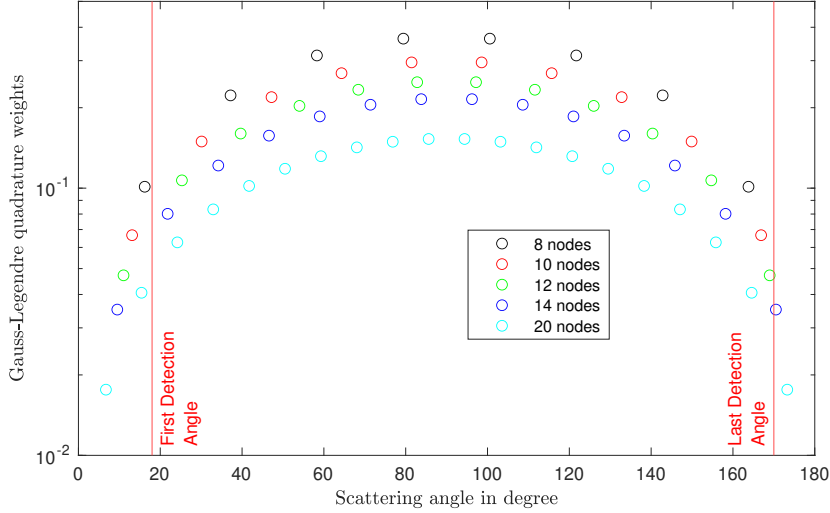


**Figure 3.** The angular detection range of PHIPS and the Gauss-Legendre quadrature weights when different number of nodes are used.

212

## 4.2 Connection with particle morphological complexity

213

214

215

As suggested by the above analysis, the decay rate of the expansion coefficients is a determining factor for the accuracy of retrieval. A natural question is, how to measure the decay rate of the expansion coefficient?

216

217

218

219

220

221

222

223

224

225

226

The decay rate of the expansion coefficient actually links to the smoothness, or the simplicity, of phase function. It has been well recognized that the morphological complexity of ice crystals, such as surface roughness, air-bubble inclusion will “smooth” the scattering phase function compared to a pristine counterpart. In modelling studies, attempts have been made to characterize these complexities, such as the distortion parameters and surface roughness parameter applied in Macke and Yang’s ray tracing codes. In addition, Gaussian random spheres can produce smooth phase functions (Muinonen et al., 1996). These metrics are largely equivalent in terms of the effects on phase function. Nevertheless, these complexity metrics are designed for light scattering simulation, not retrievable by a polar nephelometer. Hence the complexity metrics such as the distortion parameter are not applicable for accessing the accuracy of our algorithm.

It turns out that following parameter is useful to measure the decay rate of the expansion coefficient:

$$C_p = \left( \sum_{l=0}^{\infty} |\hat{c}_{GO,l}| \right)^{-1}. \quad (28)$$

227

228

229

230

231

232

233

234

235

236

In practice,  $C_p$  can only be estimated by a truncated series of Legendre polynomials. To our surprise, the value of  $C_p$  is closely related to the distortion parameter,  $\delta$ , designed for ray-tracing computation. The upper panel of Fig. 4 shows the scattering phase functions of a hexagonal columnar particle with different  $C_p$  values. As displayed in the figure, the halo produced by pristine hexagonal column corresponds to  $C_p = 0.01$ . As the value  $C_p$  increases, the halo disappears in the scattering phase function. The lower panel of Fig. 4 displays the relation between the distortion parameter and  $C_p$  for various hexagonal columns and plates, where  $R$  denotes radius and  $L$  denotes the length in  $\mu m$ . It can be seen that relation is very close to a linear proportional relation, suggesting strong correlation between the two. Therefore, the value of  $C_p$  can also be used as an indicator of

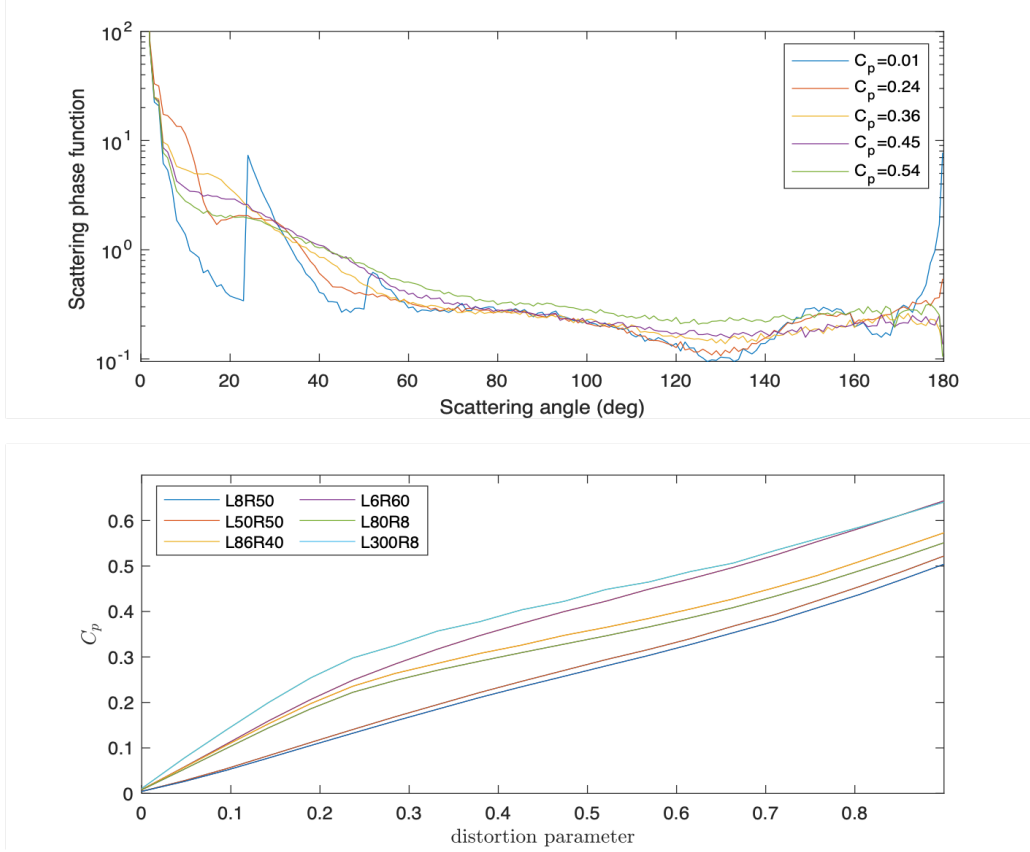


**Figure 4.** The correlation of  $C_p$  and distortion parameter applied in Macke's ray-tracing code.

237  
238

the degree of complexity of ice crystals. What being more useful in practice is that it is retrievable by a polar nephelometer.

In the following, we discuss some basic properties of  $C_p$ . For arbitrary normalized phase function,  $C_p$  satisfies the following relation:

$$0 \leq C_p \leq 1. \quad (29)$$

The values of 0 and 1 correspond to a Dirac delta function (i.e., no scattering) and isotropic scattering phase function respectively. This is due to the following relation:

$$2\delta(1 - \cos(\theta)) = \sum_{l=0}^{\infty} (2l + 1)P_l(\cos(\theta)), \quad (30)$$

meaning  $\hat{c}_{GO,l} = 1$  for all  $l$ , which makes the value of  $C_p$  infinitely close to *zero*. On the other hand, for a constant phase function, we have:

$$\hat{c}_{GO,l} = \begin{cases} 1 & \text{if } l = 0, \\ 0 & \text{if } l > 0, \end{cases}$$

which leads to  $C_p = 1$ . For the H-G phase function, we have

$$C_p = \left( \sum_{l=0}^{\infty} |g^l| \right)^{-1} = 1 - |g|. \quad (31)$$

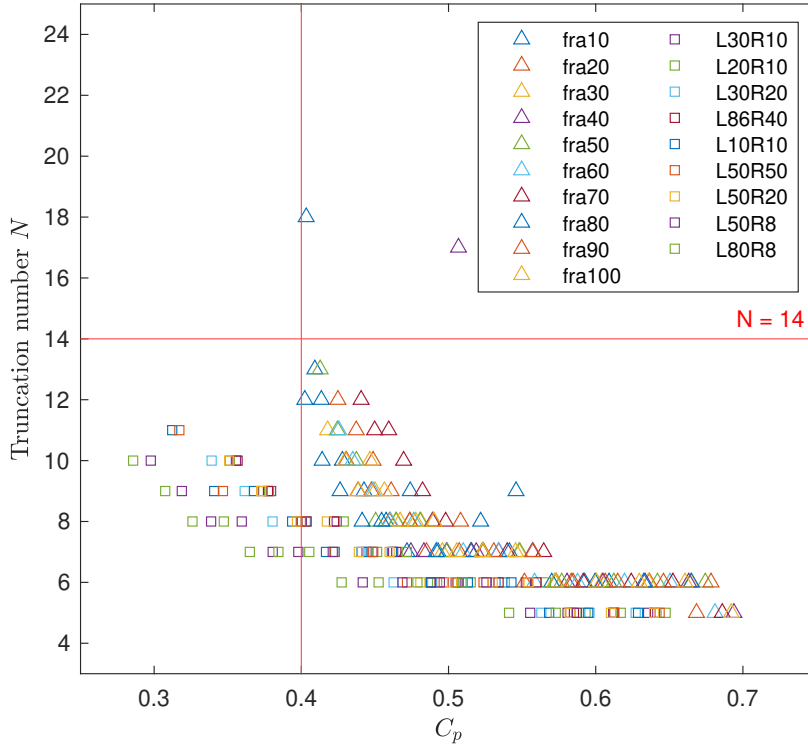


**Figure 5.** Number of truncation term  $N$  associated with truncation error  $\varepsilon = 0.001$ , as a function of  $C_p$  for different ice crystal scattering models.

239 Observe that for H-G phase function, the value of  $C_p$  is always inversely proportional  
 240 to the asymmetry parameter with constant ratio of  $-1$ , while this is not true for the scat-  
 241 tering of real ice crystals. As a matter of fact, based on simulations, the relation between  
 242  $C_p$  and asymmetry parameter  $g$  is complicated and closely related to the aspect ratio  
 243 of the particle (see Fig. 10). For aspect ratio close to unity, the asymmetry parameter,  
 244 as the first moment of the phase function, decays rather slowly in the region of small  $C_p$ .  
 245 We shall discuss this in more detailed in the next section.

246 The introduction of the auxiliary parameter  $C_p$  is an important component of our  
 247 method, because it can be simultaneously estimated with asymmetry parameter and serves  
 248 the purpose of accessing the accuracy. Fig. 5 displays the number of truncation terms  
 249  $N$  associated with an error of 0.001 (Eq. (26)), as a function of  $C_p$  for different light scat-  
 250 tering models. The legend of *fra100*, for example, denotes the model of a second gener-  
 251 ation random fractal shape with radius of  $100 \mu m$ . There are two branches of points  
 252 associated with two different models. The upper branch is associated with the *fractal*  
 253 model (denoted by *triangle*), while the lower branch is associated with the *hexagonal*  
 254 models (denoted by *square*). It can be seen that for most of the models, the number of  
 255 truncation term  $N$  is smaller than 14 as  $C_p > 0.4$ . In other words, if  $C_p$  large than 0.4,  
 256 the error of retrieval shall be at the order of 0.001.

257 Numerical experiment has been carried out to further verify this observation. For  
 258 example, in Fig. 6, the red and black curves show the true values of asymmetry param-  
 259 eter and  $C_p$  respectively, while the green and blue curves are the corresponding retrieval  
 260 values. We note that the true values are calculated based on the mixing of the six mod-

261 els used in Fig. 4. It can be seen that when  $C_p < 0.23$ , large bias could be induced. This  
 262 is because in this region, a large number of truncation term is needed to accurately rep-  
 263 resent the phase function. When  $0.23 \leq C_p \leq 0.4$ , the error of retrieval starts to con-  
 264 verge. When  $C_p > 0.4$ , the retrieval becomes highly accurate, which is consistent with  
 265 our analysis. Based on Fig. 6, we can further observe that: 1. both estimated value of  
 266 asymmetry parameter and  $C_p$  will converge to its true value; 2. the asymmetry param-  
 267 eter is generally negatively correlated with  $C_p$  as  $C_p$  becomes large enough (e.g.,  $C_p >$   
 268 0.4), and this could be used as an additional constrain for our retrieval.

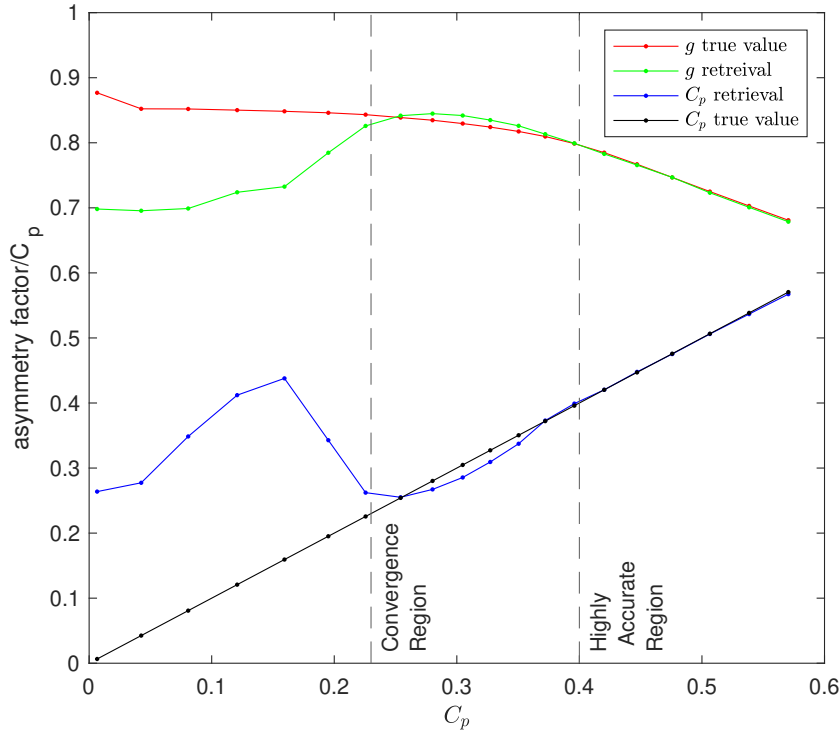


**Figure 6.**  $C_p$  and its corresponding asymmetry parameter for a mixture of different models and their retrieval results based on our method.

### 269 4.3 Other error sources

For geometric-optics treatment to be applicable, we have set a lower limit of particle size to be  $26\mu m$ , corresponding to a size parameter of 50. The error associated with this limit can be estimated by (Mishchenko et al., 2002):

$$O(x^{-3/2}) = O(50^{-3/2}) = 0.003. \quad (32)$$

270 In practice, the particle size is generally larger than this limit.

For the Gauss-Legendre quadrature to be used for integration, the intensities at the corresponding nodes must be known. Nonetheless, for many of the polar nephelometer, including PHIPS, the detectors used for measuring the intensity are often placed equally-spaced. This leads to a potential error caused by interpolation or extrapolation. Such an error is presumably small, provided that the phase function is smooth enough after averaging. To avoid potential bias of interpolation/extrapolation, we use the average value

obtained from multiple interpolation methods. Specifically,

$$I(\arccos(x_i)) = \frac{1}{3}(I_{nearest} + I_{linear} + I_{cubic}), \quad (33)$$

where  $I(\arccos(x_i))$  is the intensity to be used for Gaussian quadrature, and  $I_{nearest}$ ,  $I_{linear}$  and  $I_{cubic}$  are the interpolation intensities based on the *nearest-point*, *linear*, and *cubic* interpolation methods respectively. Numerical experiments have been carried out to verify the accuracy of the scheme (as seen in Fig. 6). It should be noted that as  $C_p$  becomes close to or larger than 0.4, the value of integration becomes rather invariant to the interpolation methods. In other words, different interpolation methods will give the same value. The extrapolation to small angles based on Eq. (33) serve the purpose of estimating the value of  $C_p$ . It is worth noting that the interpolation error could be voided if the detector is placed according to the Gauss-Legendre nodes.

In addition, we note that to avoid contamination by diffraction, the first small detection angle  $\theta_1$  should satisfy

$$\theta_1 \geq \frac{7}{x}, \quad (34)$$

where  $x$  is the particle size parameter. Assuming a lower limit of  $x = 50$ , the optimal number of nodes to be used is  $n_t = 16$  and  $\theta_1 = 8.35^\circ$ .

Apart from the error associated with the algorithm, in practice, the errors caused by instrument design, sensors, noises, data processing, could potentially be important. A discussion of these issues is beyond the scope of this paper, more information can be seen in (Baumgardner et al., 2017).

## 5 A case study of an Arctic cirrus

As an application of our method, we report the results from a case study of Arctic cirrus sampled on June 29th, 2021 during the CIRRUS in High-Latitude (CIRRUS-HL) campaign when measurements flights were made in natural and aviation influenced cirrus using the DLR HALO aircraft equipped with a suite of in-situ and remote sensing instruments. The in-situ instrumentation included the PHIPS probe for characterisation of the ice crystal angular light scattering properties. On the day of the case study, a warm front associated with southwesterly flow on the east coast of Greenland generated high level clouds north and northeast of Iceland. A thick Arctic cirrus cloud layer reaching from 8.8 km to 11.3 km was observed and sampled in-situ on six different altitudes that were langragian to the airflow. Weather forecast prior to the sampling showed ascending air masses indicating a potential liquid origin for the cirrus ice crystals.

### 5.1 Time series of temperature and ice crystal properties

Figure 7 shows a time series of the flight altitude and temperature (panel A), the ice crystal the area-equivalent diameter derived from the PHIPS stereo-microscopic images (panel B) and the corresponding values for  $C_p$  (panel C) and asymmetry parameter (panel D). Each data point in these panels represents an ensemble measurements of 20 consecutive single-particle events. It is assumed that there is no preferred particle orientation in these populations.

Largest ice crystal sizes were observed in the lowest sampling levels (between 8.8 km and 9.5 km,  $-35^\circ\text{C}$  and  $-39^\circ\text{C}$ ) where ice crystals with mean diameters up to  $182 \mu\text{m}$  were observed. Stereo-microscopic images showed that the lowest sampling levels were dominated by compact and highly irregular crystals showing plate like growth with occasional bullet rosettes embedded. Panel I in figure 8 shows example crystals from a period between 10:16:09 and 10:16:56 UTC that is highlighted with letter I in Fig. 7. The ice crystal diameter,  $C_p$  value and  $g$  are highlighted with increased symbol size in the corresponding panels. During this period 53 stereo-images of ice crystals were acquired,

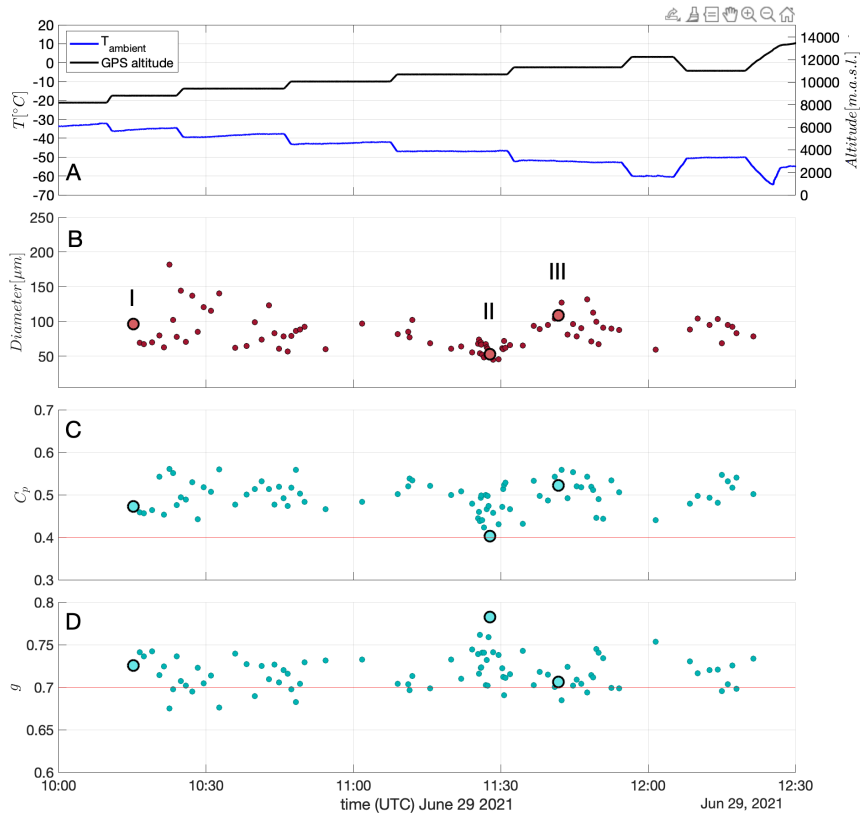


**Figure 7.** Application of the proposed method for retrieving the parameter  $C_p$  and asymmetry parameter  $g$  in CIRRUS-HL with PHIPS instrument, on June 29th, 2021. The panel A shows the ambient temperature in degree Celsius together with the GPS altitude, the panel B the mean diameter of the crystal population, the panel C the complexity parameter  $C_p$  and the panel D the values for  $g$  for the same population.

313 from which 53% were manually classified as irregular crystals, 13% as side-planes, 26%  
 314 showed indication of shattering and the rest (8%) were incompletely imaged and could  
 315 not been classified.

316 After 10:43 UTC mostly bullet rosettes and small compact crystals, that partly re-  
 317 sembled sublimated bullet rosettes, were observed. The average diameter was predom-  
 318 inantly below  $100 \mu\text{m}$ . Panel II in figure 8 shows example crystals from a period between  
 319 11:27:38 and 11:28:00 UTC, when compact and sometimes even quasi-spherical crystals  
 320 were observed. This period included 27 stereo-microscopic images, from which 41% were  
 321 manually classified as quasi-spherical crystals, 30% as bullet rosettes, 19% as irregular  
 322 and the rest (10%) could not be classified. All of the observed bullet rosettes showed in-  
 323 dications of sublimation and simultaneous RH measurements (not shown here) confirmed  
 324 occasional periods of sub-saturated conditions that might have contributed to sublima-  
 325 tion of these crystals.

326 The two highest sampling levels (around 11.3 km and  $-52^{\circ}\text{C}$ ) consisted of bullet  
 327 rosettes with varying degree of complexity. Panel III in figure 8 shows example crystals  
 328 from a period between 11:41:30 and 11:41:54 UTC, when bullet rosettes with air inclu-

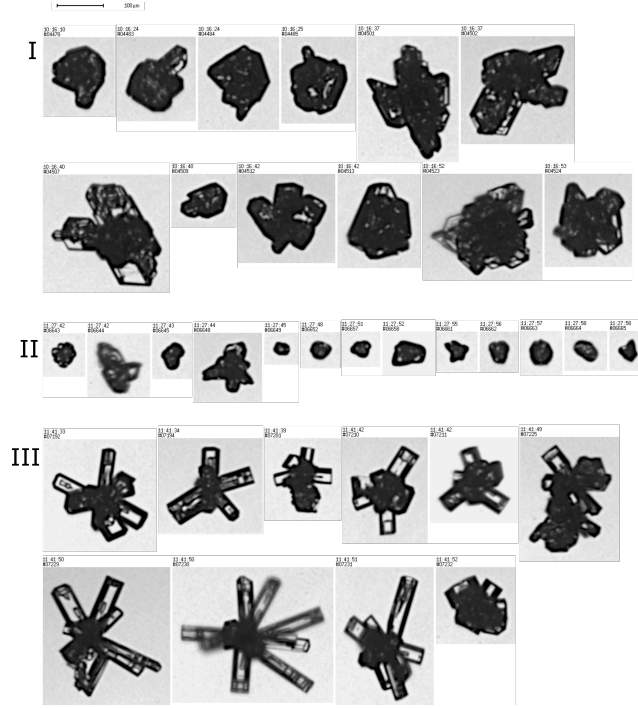


**Figure 8.** Example ice crystal images captured with the PHIPS probe from three periods shown in Fig. 7.

329 sions and hollowness were observed. This period included 51 stereo-microscopic images,  
 330 from which 78% were manually classified as bullet rosettes, 4% as irregular, 12% showed  
 331 indication of shattering, one crystal was an individual bullet and the rest (4%) could not  
 332 be classified. Later, around 11:43 UTC the bullet rosettes appeared increasing complex  
 333 with side plane growth of varying degree.

The stereo-microscopic images indicated prevailing crystal complexities in the form  
 of hollowness, surface roughness, air inclusions and polycrystallinity. This is confirmed  
 by the retrieved value of  $C_p$ , which was always above 0.4, also suggesting high accuracy  
 of the retrieval of  $g$ . In addition, the particle size is generally above  $50 \mu m$ , which cor-  
 responds to a size parameter around 295. In accordance with Eq. (32), the bias caused  
 by geometric optics ray-tracing treatment is:

$$O(x^{-3/2}) = O(295^{-3/2}) = 10^{-4}, \quad (35)$$

334 which is small enough for accurate asymmetry parameter retrieval.

335 The algorithm described in Section 3 can be also used to recover the scattering phase  
 336 function. Figure 9 displays the angular scattering function measurement and its extrap-  
 337 olation to whole angular range based on Eq. (20) for the three periods shown in Fig. 7.  
 338 Note that the measurements are scaled such that its value at 42 degree matches the nor-  
 339 malized phase function. Generally the peak of the normalized phase function will reach  
 340 to the order of  $10^5$  to  $10^6$ . The corresponding asymmetry parameter,  $g$ , and the value  
 341 of  $C_p$  are displayed in the legends. It can be seen that lower retrieved  $g$  corresponds to  
 342 a higher side- and backscattering intensity, as is expected. Because these phase functions  
 343 are from direct in-situ measurement, they are potentially useful for radiative transfer sim-  
 344 ulations.

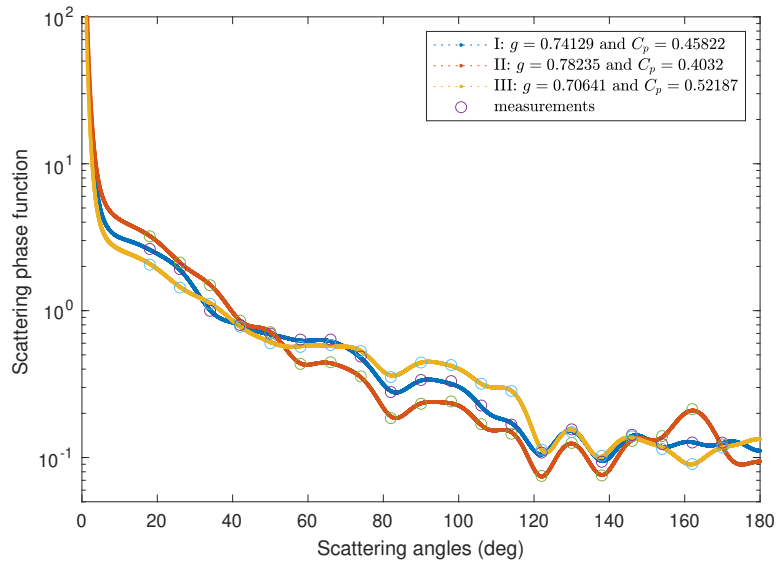


**Figure 9.** Three examples of extrapolated phase function and their asymmetry parameters and  $C_p$  values measured by PHIPS instrument, on June 29th, 2021. The measurements are indicated as open circles and are scaled to the phase function. The periods I, II and III are highlighted in Fig. 7 and example crystals corresponding to these periods are shown in Fig. 8.

345 The Figure 7D shows the retrieved values for  $g$ . Overall, the values for  $g$  vary be-  
 346 tween 0.67 and 0.78 with a median of 0.72 (Fig. 10). No clear trend in  $g$  can be seen  
 347 between the different altitudes or different crystal habits, which can be explained with the  
 348 observed complexity of the ice crystals. Only during one period  $g$  values above 0.75 are  
 349 observed. As discussed above, this period around 11:26 UTC showed small compact and  
 350 quasi-spherical ice crystals occasionally in sub-saturated conditions. Therefore, the in-  
 351 crease in  $g$  can be explained by decrease in the crystal complexity caused by sublima-  
 352 tion of the crystals.

## 353 5.2 On the $g - C_p$ relation

354 It has been well recognized that the asymmetry parameter and complexity of par-  
 355 ticle has some kinds of negative correlations. More information about the ice crystal com-  
 356 plexity can be seen in a recent review paper by (Järvinen et al., 2021) and the refer-  
 357 ences therein. This relation is worthy of study in a more quantitative way because, among  
 358 other factors (such as size), the complexity could play an important role in determin-  
 359 ing the asymmetry parameter of ice crystals. To our knowledge, such correlation has not  
 360 been described in a uniform way. A major issue is that the definition of optical complex-  
 361 ity of ice particle (model) is often dependent on specific models and methods, which makes  
 362 the comparison between different optical models rather difficult, if not impossible. Since  
 363 the asymmetry parameter is the first moment of scattering phase function, defining the  
 364 “complexity” from the phase function moments seems to be reasonable and coherent.

365 The upper panel of Figure 10 displays the relations between the retrieved asym-  
 366 metry parameter  $g$  and  $C_p$ . In total  $\sim 140$   $g - C_p$  pairs are shown, indicating a clear  
 367 negative correlation. In addition, we show the modeling curve of hexagonal particle mod-  
 368 els with different aspect ratios. The high-aspect-ratio models (very flat plates or very  
 369 long columns) correspond to those high-asymmetry-parameter curves in the low- $C_p$  re-

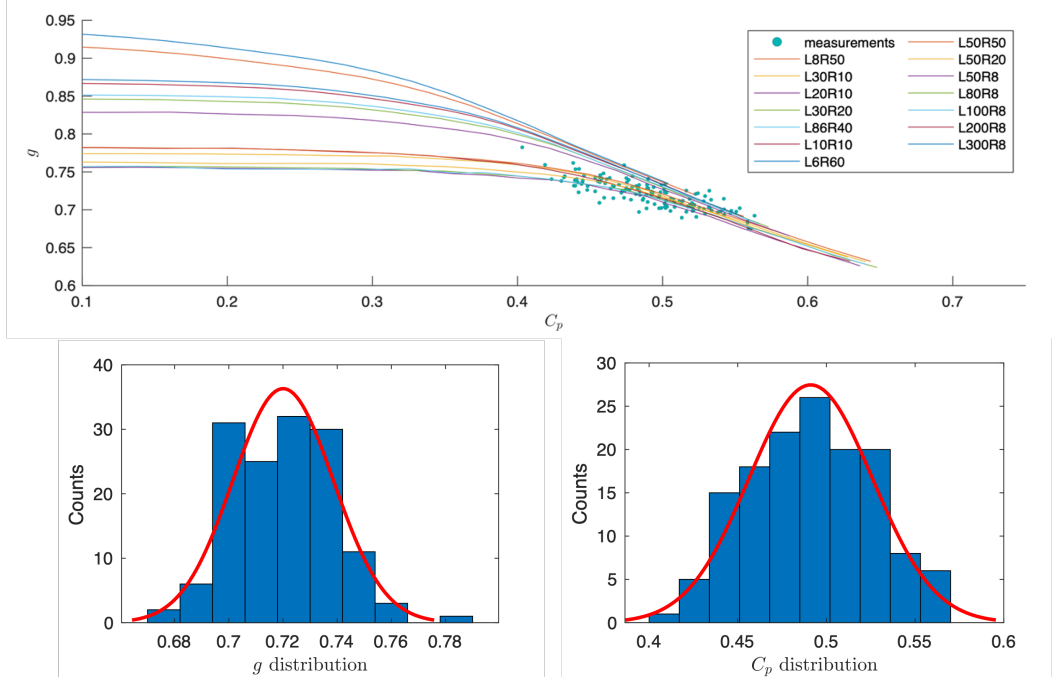


**Figure 10.** The relation between asymmetry parameter  $g$  and  $C_p$  in comparison with different scattering models. Based on data measured in CIRRUS-HL with PHIPS instrument, on June 29th, 2021

370 gion. When the aspect ratio of the hexagonal model is close to unity, the asymmetry pa-  
 371 rameter seems to be insensitive to the increase of  $C_p$ . However, when the  $C_p$  becomes  
 372 large enough, the asymmetry parameter of all particle models decreases in a similar rate.  
 373 The retrieved data points of  $g-C_p$  pairs are mostly concentrated in the high- $C_p$  region  
 374 (i.e.,  $C_p > 0.4$ ), suggesting high complexity of real ice crystals. It can be seen that the  
 375  $g - C_p$  relation from the measurement matches well with the light scattering models.

376 The lower panels of Figure 10 show the histogram fitting of asymmetry parameter  
 377 and the complexity parameter  $C_p$ , both displaying an approximate Gaussian profile.  
 378 For asymmetry parameter, the mean value is  $g = 0.7200$ , and the standard deviation  
 379 is  $\sigma = 0.0186$ , whereas the complexity parameter has a mean value of  $C_p = 0.4911$   
 380 and the standard deviation  $\sigma = 0.0348$ . The distribution of  $C_p$  suggests that our re-  
 381 sult is within the region of high accuracy.

## 382 6 Conclusions

383 Accurately obtaining the asymmetry parameter of ice crystals is important for cli-  
 384 mate modeling, numerical scattering model development and atmospheric remote sens-  
 385 ing. As a direct approach, in-situ measurements should be able to provide reliable ground  
 386 truth. To improve the accuracy, we developed a novel and stable method for retrieving  
 387 the asymmetry parameter from in-situ polar nephelometer measurements, i.e., by fitting  
 388 the measured angular scattering intensity with Legendre polynomials.

389 A key feature of the method is that it does not rely on any specific assumption about  
 390 the truncated angular range in the near-forward scattering directions – an inherent prob-  
 391 lem of nephelometer measurements. In other words, it is a light scattering model-free  
 392 approach and the asymmetry parameter is derived only based on measured data. This

393 is achieved by exploiting the fact that the forward *diffraction* and the *refraction* –  
 394 *reflection* energies are asymptotically equal. By doing so, we manage to constrain the  
 395 error of integration in accordance with the smoothness of the angular intensity distri-  
 396 bution. The theoretical basis of this approach links to the Gauss-Legendre quadrature,  
 397 which is exact provided that the scattering phase function is smooth enough. As the scat-  
 398 tering phase function becomes smooth, the nodes of Gauss-Legendre quadrature will be  
 399 very well confined in the range of detection, and the assumption on the undetectable range  
 400 become redundant. As a way of finding the best-fitting coefficients, the Gaussian inte-  
 401 gration method is both stable and accurate. For the geometric-optics treatment to be  
 402 valid, however, it is only applicable to ice crystals with a characteristic length larger than  
 403 26  $\mu\text{m}$  at a wavelength of 532  $\text{nm}$ .

404 The parameter  $C_p$  has been introduced to characterize the smoothness of the phase  
 405 function for the purpose of an error analysis. We also found a strong correlation between  
 406  $C_p$  and the distortion parameter used in the ray-tracing simulation. Therefore,  $C_p$  can  
 407 also be used as an indicator of morphological complexity of ice crystals. It is found that  
 408 as  $C_p$  reaches to 0.4, the retrieval becomes highly accurate.

409 As an application, we analyzed a case study of Arctic cirrus from the recent air-  
 410 borne campaign CIRRUS-HL where polar nephelometer measurements were conducted  
 411 using the PHIPS probe. The retrieved asymmetry parameter reveals clear negative cor-  
 412 relation with  $C_p$ . The validity of our method is evident from the fact that the magni-  
 413 tude of  $C_p$  is generally above 0.4, which belongs to the region of high-accuracy. The me-  
 414 dian asymmetry parameter around 0.72 that was deduced from this Arctic cirrus case  
 415 falls into the range between CIN measurements (Gerber et al., 2000; Garrett et al., 2001,  
 416 2003) and radiometric flux measurements (Stephens et al., 1990) (see Tab. 1). The re-  
 417 trieved value of  $C_p$  (=0.49) suggests that real ice crystals could have much more com-  
 418 plex morphology than the idealized models.

## 419 Acknowledgments

420 We would like to thank the KIT group Airborne Cloud Observations and especially Shawn  
 421 Wagner for preparing and operating the PHIPS probe during CIRRUS-HL. We also thank  
 422 DLR for flight operations during CIRRUS-HL and Vladyslav Nenakhov and Christian  
 423 Mallaun for preparing the BAHAMAS data used in Figure 7. This work was funded by  
 424 the Helmholtz Association’s Initiative and Networking Fund (grant agreement no. VH-  
 425 NG-1531).

## 426 References

- 427 Abdelmonem, A., Järvinen, E., Duft, D., Hirst, E., Vogt, S., Leisner, T., &  
 428 Schnaiter, M. (2016). Phips-halo: the airborne particle habit imaging and  
 429 polar scattering probe – part 1: Design and operation. *Atmospheric Measure-*  
 430 *ment Techniques*, 9(7), 3131–3144. doi: 10.5194/amt-9-3131-2016
- 431 Auriol, F., Gayet, J.-F., Febvre, G., Jourdan, O., Labonnote, L., & Brogniez, G.  
 432 (2001). In situ observation of cirrus scattering phase functions with 22 and  
 433 46 halos: Cloud field study on 19 february 1998. *Journal of the atmospheric*  
 434 *sciences*, 58(22), 3376–3390.
- 435 Bacon, N. J., & Swanson, B. D. (2000). Laboratory measurements of light scattering  
 436 by single levitated ice crystals. *Journal of the atmospheric sciences*, 57(13),  
 437 2094–2104.
- 438 Baumgardner, D., Abel, S., Axisa, D., Cotton, R., Crosier, J., Field, P., ... others  
 439 (2017). Cloud ice properties: In situ measurement challenges. *Meteorological*  
 440 *monographs*, 58, 9–1.
- 441 Bohren, C. F., & Huffman, D. R. (2008). *Absorption and scattering of light by small*  
 442 *particles*, p110. John Wiley & Sons.

- 443 C.-Labonnote, L., Brogniez, G., Doutriaux-Boucher, M., Buriez, J.-C., Gayet, J.-F.,  
 444 & Chepfer, H. (2000). Modeling of light scattering in cirrus clouds with inho-  
 445 mogeneous hexagonal monocrystals. comparison with in-situ and adeos-polder  
 446 measurements. *Geophysical research letters*, *27*(1), 113–116.
- 447 Diedenhoven, B. v., Cairns, B., Fridlind, A., Ackerman, A., & Garrett, T. (2013).  
 448 Remote sensing of ice crystal asymmetry parameter using multi-directional  
 449 polarization measurements—part 2: Application to the research scanning po-  
 450 larimeter. *Atmospheric Chemistry and Physics*, *13*(6), 3185–3203.
- 451 Diedenhoven, B. v., Cairns, B., Geogdzhayev, I., Fridlind, A., Ackerman, A., Yang,  
 452 P., & Baum, B. (2012). Remote sensing of ice crystal asymmetry parameter  
 453 using multi-directional polarization measurements—part 1: Methodology and  
 454 evaluation with simulated measurements. *Atmospheric Measurement Tech-  
 455 niques*, *5*(10), 2361–2374.
- 456 Fouquart, Y., Bonnel, B., & Ramaswamy, V. (1991). Intercomparing shortwave radi-  
 457 ation codes for climate studies. *Journal of Geophysical Research: Atmospheres*,  
 458 *96*(D5), 8955–8968.
- 459 Fu, Q. (2007). A new parameterization of an asymmetry factor of cirrus clouds for  
 460 climate models. *Journal of Atmospheric Sciences*, *64*(11), 4140–4150.
- 461 Garrett, T. J., Gerber, H., Baumgardner, D. G., Twohy, C. H., & Weinstock,  
 462 E. M. (2003). Small, highly reflective ice crystals in low-latitude cir-  
 463 rus. *Geophysical Research Letters*, *30*(21). Retrieved from [https://  
 464 agupubs.onlinelibrary.wiley.com/doi/abs/10.1029/2003GL018153](https://agupubs.onlinelibrary.wiley.com/doi/abs/10.1029/2003GL018153) doi:  
 465 <https://doi.org/10.1029/2003GL018153>
- 466 Garrett, T. J., Hobbs, P. V., & Gerber, H. (2001). Shortwave, single-scattering  
 467 properties of arctic ice clouds. *Journal of Geophysical Research: Atmospheres*,  
 468 *106*(D14), 15155–15172.
- 469 Gayet, J.-F., Auriol, F., Oshchepkov, S., Schröder, F., Duroure, C., Febvre, G., ...  
 470 Daugereon, D. (1998). In situ measurements of the scattering phase function  
 471 of stratocumulus, contrails and cirrus. *Geophysical Research Letters*, *25*(7),  
 472 971–974. doi: 10.1029/98GL00541
- 473 Gayet, J.-F., Ovarlez, J., Shcherbakov, V., Ström, J., Schumann, U., Minikin, A.,  
 474 ... Monier, M. (2004). Cirrus cloud microphysical and optical properties at  
 475 southern and northern midlatitudes during the inca experiment. *Journal of  
 476 Geophysical Research: Atmospheres*, *109*(D20).
- 477 Gerber, H., Takano, Y., Garrett, T. J., & Hobbs, P. V. (2000). Nephelometer mea-  
 478 surements of the asymmetry parameter, volume extinction coefficient, and  
 479 backscatter ratio in arctic clouds. *Journal of the atmospheric sciences*, *57*(18),  
 480 3021–3034.
- 481 Hu, Y.-X., Wielicki, B., Lin, B., Gibson, G., Tsay, S.-C., Stamnes, K., & Wong, T.  
 482 (2000).  $\delta$ -fit: A fast and accurate treatment of particle scattering phase func-  
 483 tions with weighted singular-value decomposition least-squares fitting. *Journal  
 484 of Quantitative Spectroscopy and Radiative Transfer*, *65*(4), 681–690.
- 485 Iaquina, J., Isaka, H., & Personne, P. (1995). Scattering phase function of bullet  
 486 rosette ice crystals. *Journal of Atmospheric Sciences*, *52*(9), 1401–1413.
- 487 Järvinen, E., Jourdan, O., Neubauer, D., Yao, B., Liu, C., Andreae, M. O., ...  
 488 Schnaiter, M. (2018a). Additional global climate cooling by clouds due to ice  
 489 crystal complexity. *Atmospheric Chemistry and Physics*, *18*(21), 15767–15781.  
 490 doi: 10.5194/acp-18-15767-2018
- 491 Jourdan, O., Oshchepkov, S., Shcherbakov, V., Gayet, J.-F., & Isaka, H. (2003).  
 492 Assessment of cloud optical parameters in the solar region: Retrievals from  
 493 airborne measurements of scattering phase functions. *Journal of Geophysical  
 494 Research: Atmospheres*, *108*(D18).
- 495 Järvinen, E., van Diedenhoven, B., Magee, N., Neshyba, S., Schnaiter, M., Delene,  
 496 D., ... Kato, S. (2021). Ice crystal complexity and link to cirrus cloud radi-  
 497 ative effect. *AGU Books*, in review.

- 498 Kristjánsson, J., Edwards, J., & Mitchell, D. (2000). Impact of a new scheme for op-  
 499 tical properties of ice crystals on climates of two gcms. *Journal of Geophysical*  
 500 *Research: Atmospheres*, 105(D8), 10063–10079.
- 501 Liou, K.-N. (1986). Influence of cirrus clouds on weather and climate processes: A  
 502 global perspective. *Monthly Weather Review*, 114(6), 1167–1199.
- 503 Liou, K.-N. (1992). Radiation and cloud processes in the atmosphere. theory, obser-  
 504 vation, and modeling p487.
- 505 Liou, K.-N. (2002). *An introduction to atmospheric radiation*. Elsevier.
- 506 Liu, C., Yang, P., Minnis, P., Loeb, N., Kato, S., Heymsfield, A., & Schmitt, C.  
 507 (2014). A two-habit model for the microphysical and optical properties of ice  
 508 clouds. *Atmospheric Chemistry and Physics*, 14(24), 13719–13737.
- 509 Macke, A., Francis, P. N., McFarquhar, G. M., & Kinne, S. (1998). The role of  
 510 ice particle shapes and size distributions in the single scattering properties of  
 511 cirrus clouds. *Journal of the atmospheric sciences*, 55(17), 2874–2883.
- 512 Macke, A., Mueller, J., & Raschke, E. (1996). Single scattering properties of atmo-  
 513 spheric ice crystals. *Journal of Atmospheric Sciences*, 53(19), 2813–2825.
- 514 Meador, W., & Weaver, W. (1980). Two-stream approximations to radiative transfer  
 515 in planetary atmospheres: A unified description of existing methods and a new  
 516 improvement. *Journal of Atmospheric Sciences*, 37(3), 630–643.
- 517 Mioche, G., Josset, D., Gayet, J.-F., Pelon, J., Garnier, A., Minikin, A., &  
 518 Schwarzenboeck, A. (2010). Validation of the calipso-caliop extinction co-  
 519 efficients from in situ observations in midlatitude cirrus clouds during the  
 520 circle-2 experiment. *Journal of Geophysical Research: Atmospheres*, 115(D4).
- 521 Mishchenko, M. I., Travis, L. D., & Lacis, A. A. (2002). *Scattering, absorption, and*  
 522 *emission of light by small particles p199-p200*. Cambridge university press.
- 523 Mishchenko, M. I., Travis, L. D., & Mackowski, D. W. (1996). T-matrix computa-  
 524 tions of light scattering by nonspherical particles: A review. *Journal of Quan-*  
 525 *titative Spectroscopy and Radiative Transfer*, 55(5), 535–575.
- 526 Muinonen, K., Nousiainen, T., Fast, P., Lumme, K., & Peltoniemi, J. (1996). Light  
 527 scattering by gaussian random particles: ray optics approximation. *Journal of*  
 528 *Quantitative Spectroscopy and Radiative Transfer*, 55(5), 577–601.
- 529 Randles, C. A., Kinne, S., Myhre, G., Schulz, M., Stier, P., Fischer, J., ... others  
 530 (2013). Intercomparison of shortwave radiative transfer schemes in global  
 531 aerosol modeling: results from the aerocom radiative transfer experiment.  
 532 *Atmospheric Chemistry and Physics*, 13(5), 2347–2379.
- 533 Schnaiter, M., Järvinen, E., Abdelmonem, A., & Leisner, T. (2018). Phips-halo: the  
 534 airborne particle habit imaging and polar scattering probe – part 2: Charac-  
 535 terization and first results. *Atmospheric Measurement Techniques*, 11(1), 341–  
 536 357. Retrieved from <https://amt.copernicus.org/articles/11/341/2018/>  
 537 doi: 10.5194/amt-11-341-2018
- 538 Shcherbakov, V., Gayet, J.-F., Jourdan, O., Minikin, A., Ström, J., & Petzold, A.  
 539 (2005). Assessment of cirrus cloud optical and microphysical data reliabil-  
 540 ity by applying statistical procedures. *Journal of Atmospheric and Oceanic*  
 541 *Technology*, 22(4), 409–420.
- 542 Shiobara, M., & Asano, S. (1994). Estimation of cirrus optical thickness from sun  
 543 photometer measurements. *Journal of Applied Meteorology and Climatology*,  
 544 33(6), 672–681.
- 545 Stackhouse Jr, P. W., & Stephens, G. L. (1991). A theoretical and observational  
 546 study of the radiative properties of cirrus: Results from fire 1986. *Journal of*  
 547 *Atmospheric Sciences*, 48(18), 2044–2059.
- 548 Stephens, G. L., Tsay, S.-C., Stackhouse Jr, P. W., & Flatau, P. J. (1990). The rel-  
 549 evance of the microphysical and radiative properties of cirrus clouds to climate  
 550 and climatic feedback. *Journal of atmospheric sciences*, 47(14), 1742–1754.
- 551 Taflove, A., & Umashankar, K. R. (1990). The finite-difference time-domain method  
 552 for numerical modeling of electromagnetic wave interactions. *Electromagnetics*,

- 553 10(1-2), 105–126.
- 554 van de Hulst, H. C. (1980). *Multiple light scattering p739*. Elsevier.
- 555 van Diedenhoven, B., Ackerman, A. S., Cairns, B., & Fridlind, A. M. (2014). A flexi-  
556 ble parameterization for shortwave optical properties of ice crystals. *Journal of*  
557 *the Atmospheric Sciences*, 71(5), 1763–1782.
- 558 Wielicki, B. A., Suttles, J. T., Heymsfield, A. J., Welch, R. M., Spinhirne, J. D., Wu,  
559 M.-L. C., ... Arduini, R. F. (1990). The 27–28 october 1986 firr ifo cirrus case  
560 study: Comparison of radiative transfer theory with observations by satellite  
561 and aircraft. *Monthly Weather Review*, 118(11), 2356–2376.
- 562 Yang, P., Bi, L., Baum, B. A., Liou, K.-N., Kattawar, G. W., Mishchenko, M. I., &  
563 Cole, B. (2013). Spectrally consistent scattering, absorption, and polariza-  
564 tion properties of atmospheric ice crystals at wavelengths from 0.2 to 100  $\mu$  m.  
565 *Journal of the Atmospheric Sciences*, 70(1), 330–347.
- 566 Yang, P., Hioki, S., Saito, M., Kuo, C.-P., Baum, B., & Liou, K.-N. (2018, Decem-  
567 ber). A Review of Ice Cloud Optical Property Models for Passive Satellite Re-  
568 mote Sensing. *Atmosphere*, 9(12), 499. doi: 10.3390/atmos9120499
- 569 Yang, P., & Liou, K. (1996a). Finite-difference time domain method for light scat-  
570 tering by small ice crystals in three-dimensional space. *JOSA A*, 13(10), 2072–  
571 2085.
- 572 Yang, P., & Liou, K. (1996b). Geometric-optics–integral-equation method for light  
573 scattering by nonspherical ice crystals. *Applied Optics*, 35(33), 6568–6584.
- 574 Yurkin, M. A., Hoekstra, A. G., Brock, R. S., & Lu, J. Q. (2007). Systematic  
575 comparison of the discrete dipole approximation and the finite difference time  
576 domain method for large dielectric scatterers. *Optics express*, 15(26), 17902–  
577 17911.